Fate of organic functionalities conjugated to theranostic nanoparticles upon their activation

Martinelli, J; Denkova, AG; Gil Arranja, A; Terpstra, BE; Zhang, W; Djanashvili, K

DOI
10.1021/acs.bioconjchem.5b00552

Publication date
2016

Document Version
Final published version

Published in
Bioconjugate Chemistry

Bioconjugate Chemistry

Article

pubs.acs.org/bc

Fate of Organic Functionalities Conjugated to Theranostic Nanoparticles upon Their Activation

Jonathan Martinelli,[†] Antonia G. Denkova,[‡] Alexandra Arranja,[‡,§] Baukje E. Terpstra,[‡] Wuyuan Zhang,[†] and Kristina Djanashvili*[,†]

[†]Department of Biotechnology, Delft University of Technology, Julianalaan 136, 2628 BL Delft, The Netherlands

[‡]Radiation Science and Technology, Delft University of Technology, Mekelweg 15, 2629 JB Delft, The Netherlands

[§]Institut Charles Sadron (CNRS), 23 Rue du Loess, 67034 Strasbourg, France

Supporting Information

ABSTRACT: Neutron activation is widely applied for the preparation of radioactive isotopes to be used in imaging and/or therapy. The type of diagnostic/therapeutic agents varies from small chelates coordinating radioactive metal ions to complex nanoparticulate systems. Design of these agents often relies on conjugation of certain organic functionalities that determine their pharmacokinetics, biodistribution, targeting, and cell-penetrating abilities, or simply on tagging them with an optical label. The conjugation chemistry at the surface of nanoparticles and their final purification often require laborious procedures that become even more troublesome when radioactive materials are involved. This study represents a thorough investigation on the effects of neutron activation on the organic moieties of functionalized nanoparticles, with special focus on $^{166}Ho_2O_3$ particles conjugated with PEG-fluorescein and PEG-polyarginine motives. Spectroscopic and thermogravimetric analyses demonstrate only a limited degradation of PEG-fluorescein upon irradiation of the particles up to 10 h using a thermal neutron flux of 5×10^{16} m^{-2} s^{-1}. Cell experiments show that the polyarginine-based mechanisms of membrane penetration remain unaltered after exposure of the functionalized particles to the mixed field of neutrons and gammas present during activation. This confirms that radiation damage on the PEG-polyarginines is minimal. Intrinsic radiations from ^{166}Ho do not seem to affect the integrity of conjugated organic material. These findings open up a new perspective to simplify the procedures for the preparation of functionalized metal-based nanosystems that need to be activated by neutron irradiation in order to be applied for diagnostic and/or therapeutic purposes.

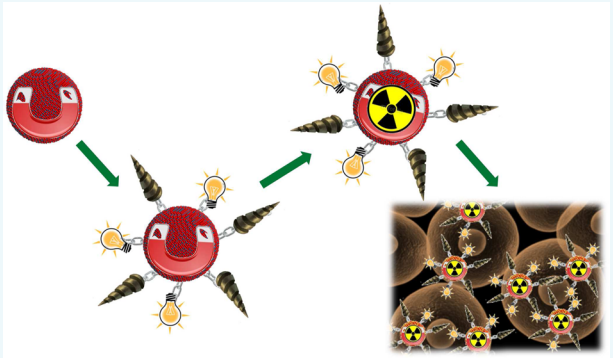

INTRODUCTION

Since its development in the 1950s, nuclear medicine has progressively grown in terms of both technical advancement and use in everyday healthcare. Nuclear medicine exploits the properties of radioactive isotopes, i.e., unstable nuclei which decay to stable atomic masses by emitting radiation (e.g., β particles). The characteristics of such emissions make certain radioisotopes suitable for diagnostics and/or therapy. The most widely used radioisotopes for diagnostic purposes are technetium-99m in single photon emission computed tomography (SPECT)[1] and fluorine-18 in positron emission tomography (PET).[2] Rubidium-82,[3] indium-111,[4] and thallium-201[5] also find some applications. Radioactive isotopes can also be exploited for therapeutic applications, and it is known that cancer cells undergoing rapid division suffer particular damage upon irradiation. Among the most relevant clinically applied radiopharmaceuticals are those based on yttrium-90,[6] samarium-153,[7] bismuth-213 and lead-212,[8] rhenium-186, rhenium-188,[9] and tin-117m.[10] Radioisotopes emitting both particles and γ rays are of particular interest in nuclear medicine, as they combine diagnostic and therapeutic abilities. The main radionuclide agents for theranostic (therapeutic and diagnostic) applications are iodine-131[11,12] and lutetium-177.[13]

In this perspective, the lanthanide holmium-166 has recently attracted interest because of its versatile properties:[14,15] as a high-energy β-emitter ($E_{\beta max}$ = 1.85 MeV) it can be exploited for cancer therapy; its low-energy γ-photons (E_γ = 81 keV) make it suitable for SPECT imaging; finally, the high magnetic moment (10.6 μB) allows its use also for magnetic resonance imaging (MRI). Furthermore, its half-life of 26.8 h is advantageous for both imaging and pharmaceutical purposes. Another advantage is that with the same probe it is possible to carry out first a preliminary evaluation of the biodistribution of the radiopharmaceutical, and then a quantitative determination of the radiation dose that can actually be delivered to diseased

Special Issue: Molecular Imaging Probe Chemistry

Received: October 12, 2015
Revised: November 24, 2015
Published: November 30, 2015

DOI: 10.1021/acs.bioconjchem.5b00552
Bioconjugate Chem. 2016, 27, 446−456

tissues taking into account lateral damage of healthy tissue. Also, the visualization by MRI is useful for medium- and long-term monitoring of the progress of the treatment. Ho-based materials represent therefore an interesting opportunity to develop theranostic systems. As an example, Ho-microspheres (activity/sphere ≤450 Bq) designed for radioembolization have already been investigated. Their in vivo biocompatibility and efficacy have been demonstrated through the successful completion of preclinical studies,[16] and the systems are currently being assessed in Phase II clinical trials.

For realistic applications, however, cancer diagnosis and treatment require efficient drug uptake and retention to the diseased site. Although the destructive effects of β particles are active even at a certain distance (maximum soft-tissue range of 8.4 mm), internalization of radioactive theranostic nanoparticles (NPs) into the target cells implies a longer residence at the site of interest, and this translates into a more effective treatment even when a lower radiation dose is applied. Therefore, smart surface functionalization is crucial to manage the behavior of the designed NPs in order to prolong blood-circulation time, reduce nonspecific delivery, and avoid leakage of toxic metal ions.[17,18] Appropriate functionalization of NPs becomes even more important for diameters smaller than 40 nm, as it is known that for tinier particles the surface chemistry is the factor determining their biodistribution and in vivo behavior, rather than the size.[19] A longer half-life of a theranostic agent in the blood pool undoubtedly brings several advantages, such as more time available for the acquisition of images and for the therapeutic effect to come into action.[20] However, when the residence becomes too long, some toxicity issues may rise depending on the materials in use, e.g., radioactive compounds. When the time of decay is relatively short (as in the case of ^{166}Ho), the material becomes quickly inert and the prolonged circulation time does not represent a risk for what the radioactivity is concerned. Targeting strategies can also offer an important solution to the problem of having potentially toxic material in the circulatory system for a long time.[21]

When the preparation of diagnostic/therapeutic materials involves neutron activation (as in the case of Ho), not only intrinsic properties (e.g., half-life of the radioisotope), but also practical aspects such as handling high activities during surface decoration of NPs and the effects of radiation on the integrity of conjugated organic functionalities have to be considered. For example, for the above-mentioned Ho-microspheres a qualitative deterioration of the polylactate coating has been reported as a consequence of their exposure to a high neutron flux.[14] The disadvantages of a post-irradiation functionalization are obvious, as it implies working with radioactive materials and special equipment and facilities, while the time available is limited by the decay of the isotope. Neutron activation of the ultimate product offers a much more elegant solution provided that it does not lead to disintegration of the organic components. To our knowledge, the latter approach does not belong to the common practice since the fate of organic moieties conjugated to nanoparticles upon neutron irradiation has never been exhaustively evaluated.

Herein we report an investigation on the effects induced by neutron activation of NPs on various conjugated organic functionalities. In fact, the possible damage would be primarily caused by the (delayed and prompt) gammas originating from the fission products of uranium in the nuclear reactor. For example, the gamma dose in the facility where the experiments described below were conducted is approximately 15 times higher than the neutron dose.[15]

The effects induced on functionalized NPs after certain irradiation times were evaluated using different analytical techniques and studied in vitro. $^{165}Ho_2O_3$ particles were additionally activated by irradiation, immediately conjugated with organic materials and left to decay in order to investigate the radiolytic effects on such moieties due to the β- and γ-emissions of ^{166}Ho.

RESULTS AND DISCUSSION

Preparation of Functionalized Nanoparticles. Polyethylene glycol (PEG) has been widely used in the past decades to functionalize the surface of nanosystems for biological applications. As hydrophilic, biocompatible polymer, PEG endows NPs with good colloidal stability, resistance to protein adsorption, long blood-circulation time, and it improves the efficacy of probes and carriers.[22] The prolonged residence time provided by PEGylation by reducing the reticuloendothelial system uptake allows theranostic systems to perform more effectively. Although a longer permanence in the blood pool also leads to concerns about toxicity, for radioactive materials this is only dependent on the decay half-life of the isotope. As mentioned above, ^{166}Ho has a half-life of about 1 day, implying that the small dose required for an injection becomes shortly inoffensive regarding the radioactivity. This is confirmed by the successful clinical trials of Ho-microspheres.[16] Moreover, from the chemical point of view, PEG offers the possibility for heterobifunctionalization,[23] thus representing a versatile tool to introduce a variety of moieties and functional groups onto the surface of NPs, such as imaging dyes and targeting vectors.

Polyarginines belong to the family of cell-penetrating peptides, known for their ability to transport various cargoes across the cell membranes.[24,25] Conjugation of these functional molecules to the surface of NPs as terminal moieties of PEG-chains provides the particles with cell-penetration potential. Additionally, application of fluorescein-terminated PEG affords the possibility not only to visualize the particles by confocal microscopy, but also to quantify spectrophotometrically the amount of conjugated organic molecules on the surface of NPs. For this study we have exploited (i) silica and (ii) holmium oxide NPs functionalized with the above-mentioned PEG-derivatives. SiO_2 was used to prepare model particles to study the effect of associated neutron and gamma radiations on the organic decorations, while Ho_2O_3-based systems allowed investigation of whether any damage occurs to conjugated PEGs by the intrinsic emissions from ^{166}Ho.

Monodispersed silica NPs were prepared according to the Stöber methodology.[26] by stirring tetraethylorthosilicate in aqueous solution of ethanol in the presence of ammonium hydroxide. The images (Figure S1a) acquired by transmission electron microscopy (TEM) show monodispersed spheres with an average diameter of about 40 nm. Addition of *N,N*-dipropargyl-3-aminopropyl-trimethoxysilane (synthesized by adapting a reported procedure for an analogous compound)[27] to the reaction mixture led to SiO_2 particles with C−C triple bonds on their surface (Si−Y). The size of the Si−Y NPs was determined by dynamic light scattering (DLS) measurements and resulted in a hydrodynamic diameter of 75 nm, while their ζ-potential amounted to −44 mV (Table 1). Ho_2O_3 NPs were prepared according to a miniemulsion-based method;[28] their TEM pictures (Figure S1b) reveal smooth round-shaped particles ca. 60 nm in diameter. Ho−Y NPs were obtained

DOI: 10.1021/acs.bioconjchem.5b00552
Bioconjugate Chem. 2016, 27, 446−456

Table 1. Properties and Applied Treatment of Si- and Ho-Based NPs Investigated in This Study

sample	diameter (nm)	ζ-potential (mV)	treatment[a]
Si−Y	75 ± 16	−44 ± 10	I + P
Si-PEG-Flu	80 ± 28	−39 ± 9	I
Si-PEG-Flu5%	77 ± 37	−24 ± 9	C
Si-PEG-Flu-Arg	76 ± 22	−35 ± 10	I
Ho-Y	67 ± 13	−1 ± 6	P, I + P
Ho-PEG-Flu	61 ± 16	−15 ± 8	C

[a]I = Irradiation, P = PEGylation, C = Control.

via condensation between *N,N*-dipropargyl-3-aminopropyl-trimethoxysilane and the OH-groups on the surface of Ho_2O_3 particles to form stable Ho−O−Si bonds. The average hydrodynamic size resulted 67 nm, while they became almost electrically neutral (Table 1).

The synthesis of modified PEGs is shown in Scheme 1. α-Azido-ω-hydroxy-PEG_{1450} (**1**) was obtained via monotosylation of PEG in the presence of Ag_2O as reported in the literature[31] and successive substitution with sodium azide. α-Azido-ω-fluorescein-PEG_{1450} (PEG-Flu) was prepared by activation of α-azido-ω-hydroxy-PEG_{1450} as the corresponding alkoxide with sodium hydride, followed by reaction with fluorescein isothiocyanate. α-Azido-ω-nonaarginine-PEG_{1450} (PEG-Arg) was synthesized following a solid-phase synthetic protocol involving the attachment of nine arginine residues to Rink amide resin through Fmoc-strategy, successive peptide-coupling with α-azido-ω-carboxy-PEG_{1450} (**3**), and final cleavage of the desired compound from the resin with trifluoroacetic acid, which also deprotects the arginine's side guanidine moiety. α-Azido-ω-methoxy-PEG_{1450} (PEG-OMe) was achieved from PEG_{1450} monomethyl ether as described above.

Functionalization of nanoparticles was carried out via copper(I)-catalyzed azide−alkyne cycloaddition reaction (CuAAC) between Si−Y or Ho−Y and the appropriate composition of PEGs using $(PPh_3)_3CuBr$ as catalyst.[29,30] For example, the particles bearing both fluorescein and polyarginine (Si-PEG-Flu-Arg) were prepared by mixing a certain amount of Si−Y with the same total amount of PEGs, of which 5 wt % consisted of PEG-Flu, 10 wt % of PEG-Arg, and the remaining 85 wt % of PEG-OMe (Scheme 2). When doing this, it was approximated that all PEGs had the same average molecular weight.

The obtained systems were initially characterized by measuring their hydrodynamic size and charge, as mentioned before for the alkynylated silica and holmium oxide. It was expected that the functionalization of the particles had no significant effect on their size: the length of a stretched PEG chain (brush conformation) with an average molecular weight of 1450 Da is about 100 Å (10 nm). However, due to their low superficial density on the NPs, the chains fold several times (mushroom conformation), thus contributing to the total size of the particles by only a few nanometers or even less. As a confirmation of this, the measured hydrodynamic diameters remained constant around 80 (Si-particles) or 65 (Ho-particles) nm. For the latter in particular, the apparent slight decrease from 67 nm (nonfunctionalized) to 61 nm (functionalized) is in fact contained and counterbalanced by the standard deviation values. Similarly, the measured ζ-potential values of the Si-based systems showed negligible variations. In this

Scheme 1. Synthesis of PEG-Derivatives for the Functionalization of Si−Y and Ho−Y via CuAAC[a]

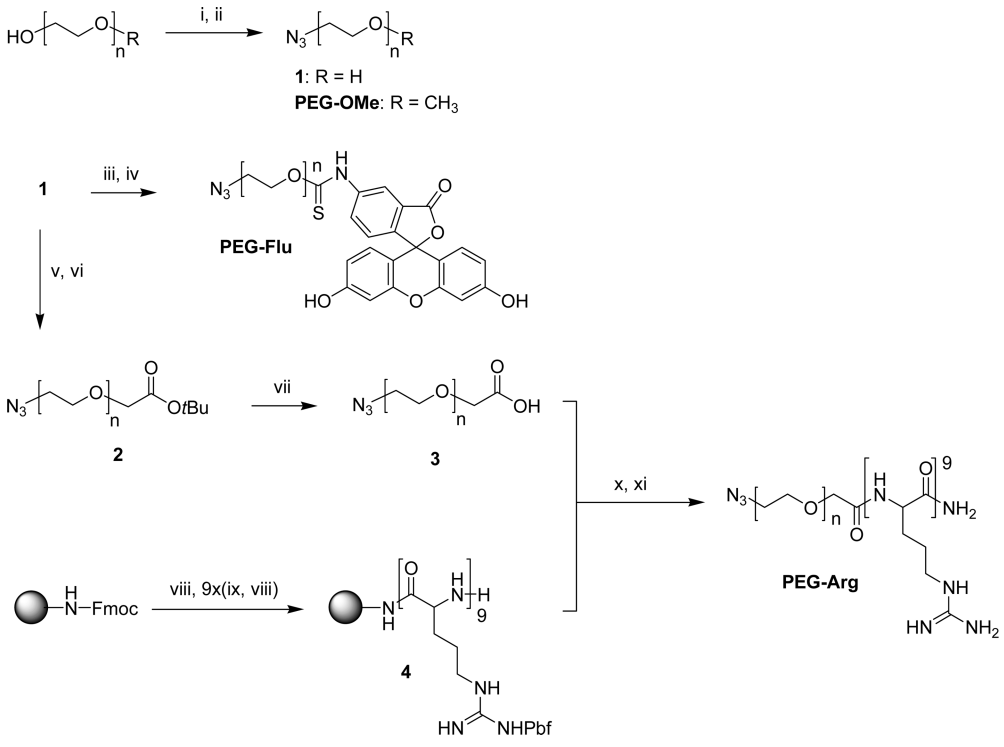

[a](i) Ag_2O, KI, TsCl, toluene, rt, 18 h; (ii) NaN_3, DMF, 90 °C, 18 h; (iii) NaH, THF, rt, 30 min; (iv) FITC, rt, 18 h; (v) NaH, DMF, 0 °C, 30 min; (vi) $BrCH_2COOtBu$, rt, 18 h; (vii) TFA, rt, 2 h; (viii) 20% piperidine in DMF, rt, 3 h; (ix) Fmoc-Arg(Pbf)-OH, HOBt, HBTU or HATU, DIPEA, DMF, rt, 3 h; (x) HOBt, HATU, DIPEA, DMF, rt, 18 h; (xi) 95:2.5:2.5 TFA/$(iPr)_3SiH/H_2O$, rt, 3 h.

DOI: 10.1021/acs.bioconjchem.5b00552
Bioconjugate Chem. 2016, 27, 446−456

Scheme 2. Attachment of PEG-Derivatives to the Surface of Alkyne-Bearing Silica NPs via CuAAC[a]

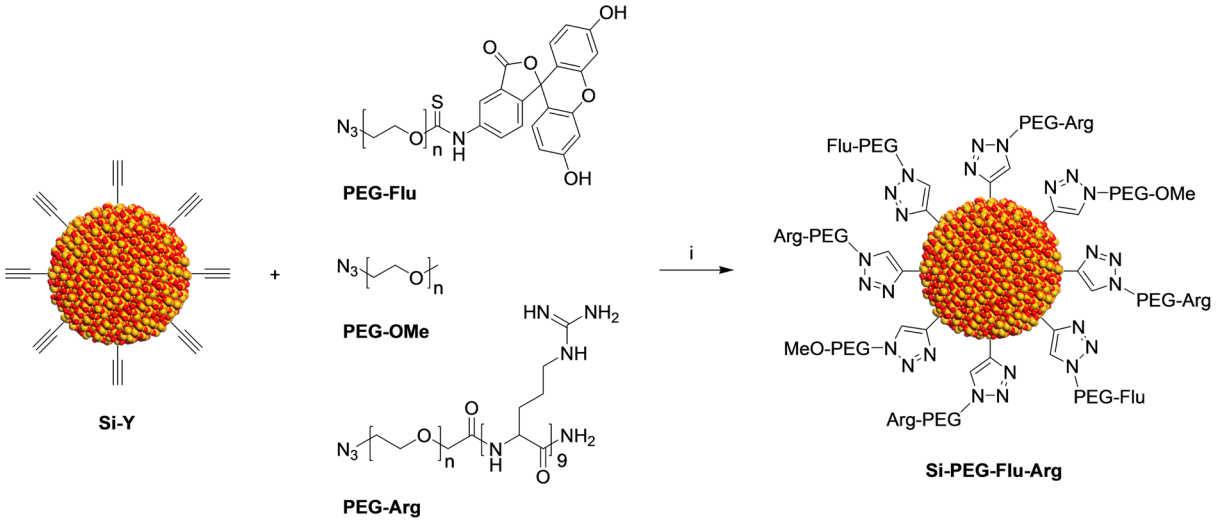

[a](i) $(PPh_3)_3CuBr$, Et_3N, THF, rt, 24 h. The same approach was applied for the functionalization of Ho–Y NPs; the final composition of organic moieties on the surface of NPs varies in accordance to the experimental approach.

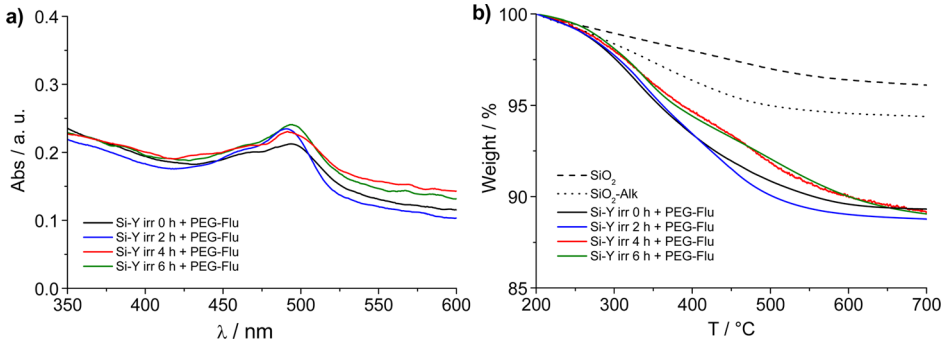

Figure 1. Characterization of NPs after neutron irradiation of Si–Y followed by their functionalization with PEG-Flu: (a) UV spectra relative to aqueous suspensions (0.1 mg mL^{-1}); (b) normalized thermogravigrams (200–700 °C).

respect, the effect of the introductions of positively charged arginines was limited by their low amount.

The composition of the functionalized NPs was confirmed by fluorescence measurements to assess the relative amount of PEG-Flu. Two different systems were prepared by using either 100 wt % PEG-Flu (Si-PEG-Flu) or 5 wt % PEG-Flu and 95 wt % of PEG-OMe (Si-PEG-Flu5%). As expected, the latter particles exhibited a fluorescence equal to about 5% of the former particles (Figure S2 and Table S1).

In order to exclude the possibility of nonspecific adsorption of PEGs on the surface of NPs, two parallel experiments were carried out where PEG-Flu was stirred with Si–Y particles under the same reaction conditions, but either in the presence or in the absence of Cu^I-catalyst. Subsequent washings and dialysis ensured the removal of unreacted organic material and the amount of PEG-Flu was determined by fluorescence measurements. The amount of fluorescein on the particles resulting from the noncatalyzed reaction corresponded to 1.8% of that from the Cu^I-catalyzed procedure (Figure S5), and therefore the nonspecific absorption of PEG-Flu at the surface of Si–Y NPs can be considered as negligible.

Neutron Irradiation of Functionalized Nanoparticles. Model silica NPs decorated with suitably modified PEG-chains were exposed to a neutron flux typically used in the preparation of ^{166}Ho microspheres for a comparable amount of time to reach activities that are typically used in radionuclide therapy (GBq range). It is noteworthy that the activity required for therapy is about 3 orders of magnitude higher than that required for imaging (GBq vs MBq). Additionally, the particular therapeutic dose depends on the type of tumor and the route of administration (i.e., intratumoral vs intravenous), and this in turn determines the amount of particles to be injected. To assess possible detrimental effects of neutron and associated gamma radiations on the organic functionalities, both fully conjugated silica NPs as well as their alkyne-bearing precursors Si–Y were exposed to a thermal neutron flux of 5×10^{16} m^{-2} s^{-1} for different time intervals up to 10 h. A 10 h irradiation at this flux results in an activity of 4 GBq when 15 mg of Ho are being used, which is comparable to activities applied in radionuclide therapy such as in the treatment of neuroendocrine tumors (i.e., 7.4 GBq of ^{177}Lu). Naturally, the activity necessary for treatment with ^{166}Ho might differ from the one used for ^{177}Lu as the two radionuclides have different radiation doses, but it is expected to be in the same order of magnitude.

The transmittance of the C≡C stretching band at ca. 2100 cm^{-1} is too weak to be observed in the IR spectra of alkyne-bearing nanoparticles, and the typical band relative to the stretching of the C_{sp}-H bond at ca. 3300 cm^{-1} is covered by the broad signal due to silanol groups and residual water (Figure

DOI: 10.1021/acs.bioconjchem.5b00552
Bioconjugate Chem. 2016, 27, 446–456

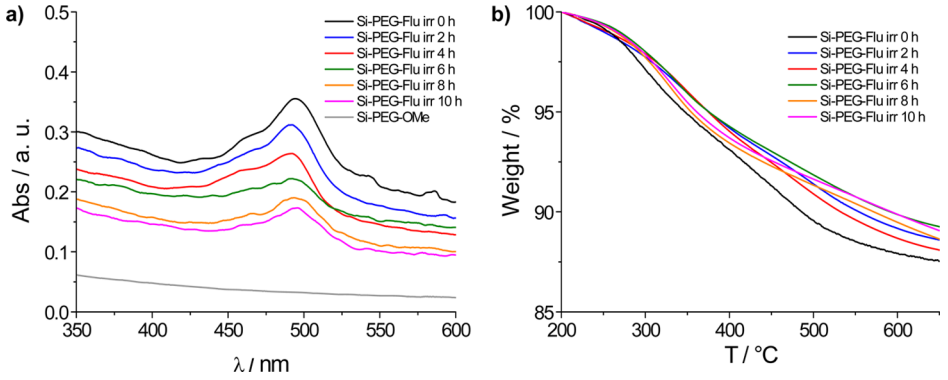

Figure 2. Evaluation of organic moieties on Si-PEG-Flu NPs after neutron irradiation for different time intervals: (a) UV spectra relative to water suspensions (0.1 mg mL^{-1}); (b) normalized TGA profiles (200−700 °C) relative to nonirradiated and irradiated Si-PEG-Flu NPs after dialysis.

S6). The amount of alkyne-groups remaining on the surface of Si−Y particles after irradiation was therefore evaluated in indirect ways. In particular, particles irradiated for different time intervals were subjected to CuAAC with PEG-Flu. The final number of PEG-Flu chains conjugated to the particles was assumed to be directly proportional to the alkyne groups which survived irradiation. UV−vis spectroscopy was used to determine the amount of PEG-Flu before and after exposure of the NPs to the neutron flux. For UV analyses, an initial suspension (0.1 mg mL^{-1}) of each system was successively diluted and the relative spectra were recorded (Figure S3). The absorbance (Abs) values at 490 nm were plotted against the corresponding concentrations to obtain straight lines (Figure S4), and the R^2 of such plots confirmed the validity of the measurements. For the calculation of the PEG-loading on the particles, it is preferable to use Abs values obtained under high dilution conditions, when interactions between chromophores are less likely to affect the absorption behavior. The UV spectra of the Si-PEG-Flu particles prepared from Si−Y irradiated for 2, 4, and 6 h clearly shows that roughly the same amount of PEG-Flu had been conjugated (Figure 1a). By using the Abs values at 490 nm for the suspensions at low concentrations with the calibration curve obtained for PEG-Flu at the same wavelength (Figure S7), an average 13% PEG-loading was determined for all systems (Table S2).

Thermogravimetric analysis (TGA) was applied to quantify the degree of functionalization in terms of weight percentage of the organic material on the surface of the inorganic NPs with respect to the total mass. The plots presented in Figure 1b are normalized at 200 °C as the loss in weight between 25 and 200 °C is basically due to physisorbed water; after that, PEG undergoes degradation. The analysis of the curves for the four systems reveals that basically no difference in organic content exists between the particles. An average loss of about 7% was calculated with respect to the naked Si-NPs (Table S3). The difference between this result and the one obtained from the UV data (~8%) is due to the fact that the latter are affected by scattering; the value assessed by TGA is to be considered more reliable. These outcomes confirm that no significant damage of triple bonds at the surface of silica NPs occurs after neutron irradiation up to 6 h.

The next step involved the investigation of the effects induced during irradiation on more complex functionalities. A batch of Si-PEG-Flu was prepared and then irradiated for the same time intervals (0, 2, 4, 6 h), and additionally 8 and 10 h. The content in terms of fluorescent moieties was first qualitatively checked by UV spectroscopy: the resulting absorption spectra (Figure 2a) demonstrate a gradual decrease of chromophore (fluorescein) activity as the absorbance at 490 nm decreases upon increase of irradiation time.

The radiation damage effects were further assessed by processing fluorescence data. An excitation wavelength of 470 nm was used, and the corresponding emission at 517 nm was recorded (Figure S8a). The fluorescence decrease obtained by peak heights and peak area (Table 2) were plotted against the irradiation time and fitting of the data was carried out (Figures 3 and S8b).

Table 2. Absorbance (490 nm) and Fluorescence (517 nm) Decrease for Si-PEG-Flu NPs (0.1 mg mL^{-1}) after Neutron Irradiation for Different Time Intervals[a]

	UV		fluorescence[d]				TGA
irradiation time (h)	Abs[b] (a.u.)	Loss[c] (%)	Height (a.u.)	Loss[c] (%)	Area (a.u.)	Loss[c] (%)	Loss[e] (%)
0	0.35	-	1.09	-	52.18	-	7.0
2	0.31	11	0.61	44	29.58	43	6.1
4	0.26	25	0.42	62	20.07	62	6.6
6	0.22	37	0.21	81	9.96	81	5.5
8	0.19	46	0.16	85	7.67	85	6.3
10	0.16	54	0.12	89	5.98	89	6.1

[a]TGA data (700 °C) are also reported for comparison. [b]λ_{max} = 490 nm. [c]λ_{ex} = 470 nm, λ_{em} = 517 nm. [d]With respect to the nonirradiated (0 h) sample. [e]With respect to Si−Y.

An exponential decrease of fluorescence is in agreement with the data observed by UV spectroscopy demonstrating that

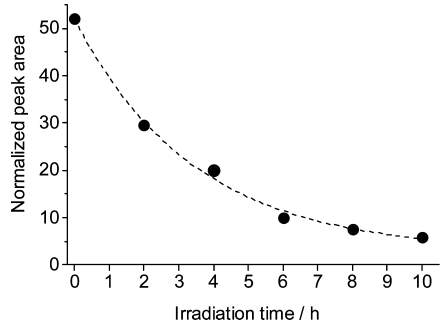

Figure 3. Areas of the peak at 517 nm in the emission spectra (λ_{ex} = 470 nm) obtained for different PEG-Flu particles (0.025 mg mL^{-1} in H_2O).

DOI: 10.1021/acs.bioconjchem.5b00552
Bioconjugate Chem. 2016, 27, 446−456

irradiation damages fluorescent moieties by about 40% per each 2 h, leaving 20% of UV activity after 6 h of irradiation.

As previously mentioned, the fluorescence values are lower than those obtained by UV because the latter method is considerably affected by scattering. The deposited radiation energy is not sufficient to break σ-bonds of the PEG-chains without affecting the fluorescein molecules; thus, it was hypothesized that the degradation only concerned the electronic system of the dye. This was confirmed by carrying out dialyses of the particles after irradiation (to remove hypothetically cleaved PEG-fragments) and comparing their TGA profiles: the thermogravigrams of Si-PEG-Flu irradiated for 10 h show a total weight-% loss at 700 °C of 88.42% before dialysis and 88.32% after dialysis, with only a 0.1% difference (Figure S9).

In addition, PEG-Flu was irradiated for 6 h under the same conditions as those used for the particles, and its ^{1}H NMR spectrum was compared with that recorded before irradiation. Changes were observed particularly in the low field region were aromatic protons resonate (Figure S10), thus proving that the gamma radiations affect the π-electronic system of fluorescein.

As demonstrated in Figure 2b, no substantial difference in organic loading was found between the particles before and after irradiation, confirming that no cleavage of material took place as a consequence of the exposure to the neutron and gamma flux present in the reactor pool. These results are quite different than those reported by Vente et al.[17] who studied the damage induced during neutron activation of ^{165}Ho enclosed in polylactic acid microspheres revealing that, at the same neutron flux, the organic material deteriorates after approximately 6 h of neutron activation. To show the importance of various irradiation parameters (e.g., time, amount, water content, material of the vial, distance from the core, neutron flux) it is useful to report that Mumper et al.[32] produced 1.3 GBq by irradiation of 50 mg of Ho-microspheres for 3 h under a flux of 9×10^{16} m^{-2} s^{-1}, while Nijsen and co-workers[16] obtained 20 GBq with a 1 h activation of 400 mg of microspheres in a flux of 5×10^{17} m^{-2} s^{-1}. In the latter case, a major deterioration of the polylactate coating was observed when more than 200 mg of material were exposed to the high neutron flux for at least 2 h, especially in the presence of water. On the contrary, when only 10 mg of microspheres were irradiated no loss of structural integrity was observed.

The possible radiolytic effects of β- and γ-radiation emitted by ^{166}Ho nuclei were also investigated using Ho_2O_3 NPs functionalized with PEG-Flu immediately after neutron activation for 2 h. This time was chosen as an acceptable compromise in order to avoid working with very high activities or waiting a long time for ^{166}Ho to decay. The activity and therefore the radiation dose due to the β- and γ-emission of ^{166}Ho are in this case lower than what is typically used in patient treatments, but they still do provide an indication of the stability of the conjugated moieties. In addition to this, the radiation dose generated by the particles is certainly expected to be lower than the dose to which they are exposed during irradiation originating from prompt and delayed gammas (>250 kGy h^{-1}).

After their assembly, ^{166}Ho-PEG-Flu particles were allowed to decay for 4 days, corresponding approximately to 4 half-life times, suspended in water via sonication for 60 min to ensure full dispersion, and their UV spectrum was acquired. Non-radioactive ^{165}Ho-PEG-Flu NPs were also prepared and their UV spectrum was compared to the previous one shown to be identical (Figure 4). This proves that the organic functionalities did not suffer any destructive effect from the radiations emitted by ^{166}Ho as a consequence of its decay to stable ^{166}Er.

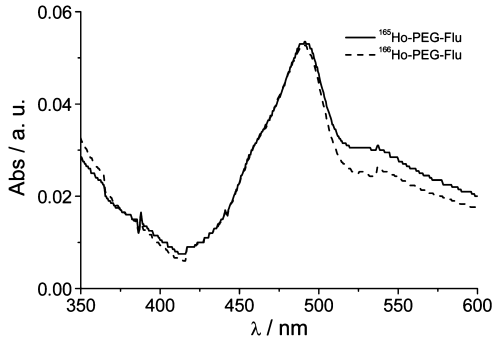

Figure 4. UV spectra of $^{165}Ho_2O_3$ and $^{166}Ho_2O_3$ particles (0.1 mg mL^{-1} in H_2O) functionalized with PEG-Flu.

Cell Experiments with Irradiated Si-PEG-Flu-Arg Nanoparticles. The final test involved the evaluation of possible damage sustained by polyarginine residues conjugated to the particles. Also, these experiments were carried out on model SiO_2 particles (Si-PEG-Flu-Arg) functionalized with PEG-Flu (5 wt %) and PEG-Arg (10 wt %) prepared as previously described. Control Si-PEG-Flu NPs with 5 wt % PEG-Flu and 95 wt % PEG-OMe were also synthesized. The characterization of such systems is reported above. A portion of the particles functionalized with PEG-Arg was irradiated for 2 h and another portion for 4 h. Because these irradiation times were enough to observe some degradation effects on conjugated PEG-Flu, they were considered appropriate for the same kind of investigation on PEG-Arg. The possible damages suffered by arginine-residues as a consequence of radiation were examined by incubating HeLa cells with irradiated or nonirradiated particles and then assessing the differences in their internalization by confocal microscopy (Figure 5).

We observed that NPs, with and without arginine-residues, were internalized by HeLa cells. However, as expected the amount of NPs internalized was much higher when NPs were functionalized with the arginine-based penetrating peptides (Figure 5, top), confirming the ability of oligo-arginines to increase NPs transport across the cell membranes.

No significant differences were observed in the internalization of NPs bearing irradiated arginines in comparison to nonirradiated analogous moieties (Figure 5, bottom). Thus, the tested irradiation times (2 and 4 h) did not damage PEG-Arg functionalities sufficiently enough to affect the interaction between particles and cells. The green fluorescence observed was mainly present in localized fluorescent spots dispersed in the cytoplasm.

Since this can be an indication of accumulation of NPs in endocytic compartments, a more precise analysis of the localization of the nanosystems within cells (Figure 6) was obtained by labeling the lysosomes with a red fluorescent probe that accumulates in acidic organelles. After incubating cells with Si-PEG-Flu-Arg particles in the presence of Lysotracker for 1 h at 37 °C, the corresponding confocal images (Figure 6) showed the colocalization (yellow areas) of the NPs with the lysosomes, suggesting that the intracellular transport of the NPs is processed via the endosomal-lysosomal pathway.

DOI: 10.1021/acs.bioconjchem.5b00552
Bioconjugate Chem. 2016, 27, 446−456

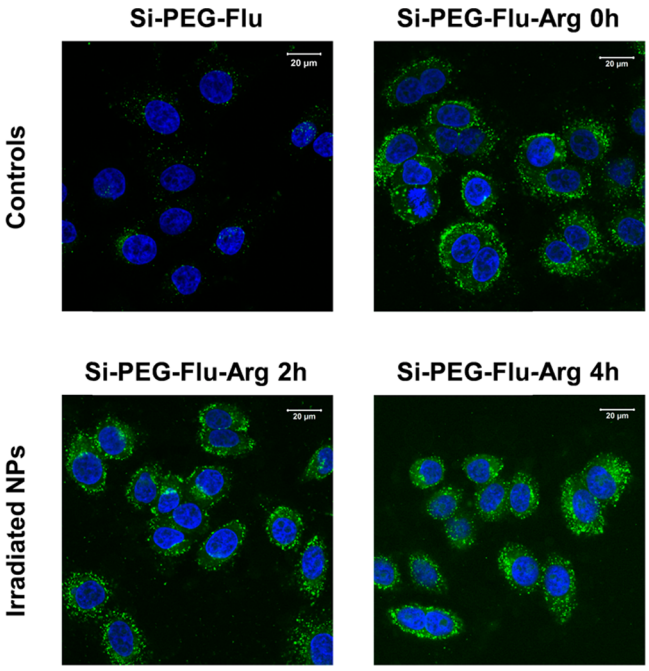

Figure 5. Effect of particle irradiation on cellular internalization. Confocal images of HeLa cells incubated with Si-PEG-Flu and Si-PEG-Flu-Arg particles irradiated for 0, 2, or 4 h, at a final concentration of 100 μg mL^{-1}. The cell nuclei were stained with DAPI. Scale bar is 20 μm.

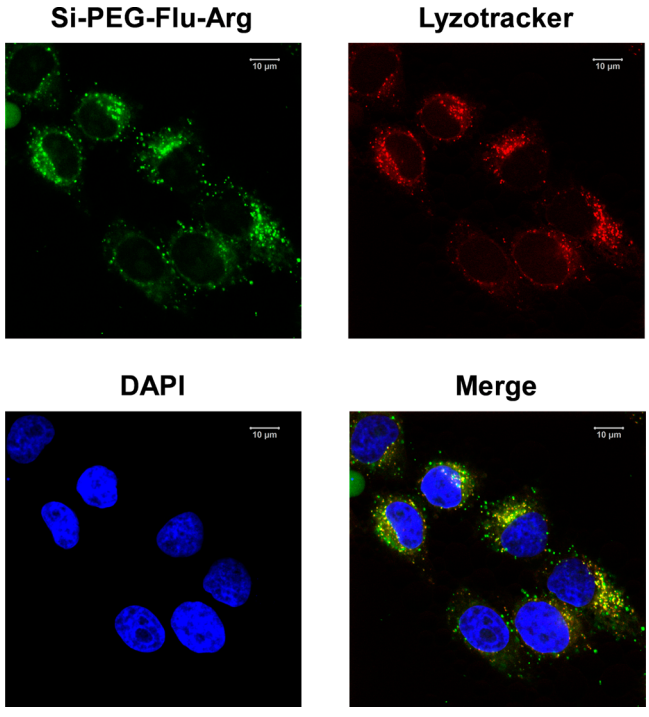

Figure 6. Internalization and intracellular localization of nonirradiated Si-PEG-Flu-Arg particles in HeLa cells after incubation for 1 h with the NPs (100 μg mL^{-1}) followed by labeling of the lysosomes with LysoTracker Red. The cell nuclei were stained with DAPI. Scale bar is 10 μm.

CONCLUSIONS

According to our investigations, C−C triple bonds are not affected by neutron irradiation up to 6 h at a flux of 5 × 10^{16} m^{-2} s^{-1}. More complex organic functionalities (π-systems), such as fluorescein moieties, were only partially damaged even after a prolonged exposure. On the contrary, polyarginines are not shown to be affected in a relevant way by radiation as they seem to retain their ability to promote cell internalization with the same effectiveness. In addition, intrinsic radioactivity from betas and gammas of ^{166}Ho activated for 2 h (~0.3 GBq) was shown to have no effect on organic functionalities. These results are particularly important in view of the assembly of hybrid organic/inorganic materials that require neutron activation, such as holmium-based nanoparticles and other suitable radiochemical systems for diagnostics and therapy that have to be functionalized with organic moieties in order to acquire defined properties (e.g., targeting or improved internalization capability). If limited damage of functional moieties occurs, the amount of such functionalities can be easily increased in order to circumvent the loss of efficiency. Our study opens up the possibility to build decorated particles entirely before irradiation and then proceed to the activation with a limited and acceptable alteration of certain functionalities.

EXPERIMENTAL SECTION

Materials and Methods. All chemicals were used as supplied from commercial sources (Alfa-Aesar, Sigma-Aldrich). "H_2O" refers to high purity water with conductivity of 0.04 μS cm^{-1}, obtained from a Milli-Q purification system. Holmium oxide particles were prepared as reported elsewhere.[28] Thin-layer chromatography (TLC) was carried out on silica plates (silica gel 60 F254, Merck 5554) and visualized by UV lamp (254 nm) or stained in $KMnO_4$, ninhydrin, or bromocresol green as appropriate. Preparative column chromatography was carried out using silica gel (Merck Silica Gel 60, 230 ± 400 mesh) presoaked in the starting eluent. Dialyses were performed using Spectra/Por Float-A-Lyzer G2 cellulose ester dialysis devices (SpectrumLabs), MWCO 100 kDa, volume 10 mL; the membranes were thoroughly rinsed with water before use. Ultrasonication was carried out by using a Qsonica Sonicator (500 W, 1/2 in. tip, 80% amplitude, time interval 0.5 s). UV measurements were performed on a Shimadzu UV−Vis spectrophotometer UV-2401 PC, with disposable plastic cuvettes of 3 mL in volume. The spectra of the irradiated Ho particles were recorded on a Shimadzu UV-1601 at Reactor Institute Delft. Fluorescence data were acquired on a JASCO J-815 CD Spectrometer. Thermogravimetric analyses were conducted by using a PerkinElmer Thermogravimetric Analyzer TGA7 equipped with a Thermal Analysis Controller TAC 7/DX, from 25 to 900 °C (10 °C min^{-1}) under air atmosphere. DLS experiments were carried out by using a Malvern Zetasizer NanoZS operating in a particle size range from 0.6 nm to 6 μm and equipped by a laser He−Ne with λ = 633 nm. The measurements were performed at 25 °C, and the average diameter was based on three individual measurements, 20 scans for each measurement. TEM analyses were performed on a JEOL JEM-2100 transmission electron microscope. Samples of nanoparticles from dilute aqueous dispersions were evaporated over a 400-mesh copper measurement grid. The instrument operated at an accelerating voltage of 200 kV for the acquisition of section images. ^{1}H and ^{13}C NMR was performed on Agilent MR400DD2 spectrometer operating at 400 MHz, 25 °C. Samples were prepared in 5 mm NMR tubes by dissolving the compounds in appropriate deuterated solvents. Chemical shifts are reported in ppm, relative to TMS as internal standard, and

DOI: 10.1021/acs.bioconjchem.5b00552
Bioconjugate Chem. 2016, 27, 446−456

coupling constants in Hz. Splitting patterns are described as singlet (s), broad singlet (bs), doublet (d), double doublet (dd), triplet (t), quartet (q), multiplet (m), or broad multiplet (bm). IR spectra were recorded in the range 4000−400 cm^{-1} at 4 cm^{-1} resolution using a Thermo Nicolet 6700 FT-IR spectrometer.

Synthesis of PEG-Derivatives. *α-Tosyl-ω-hydroxy-PEG_{1450}.* PEG_{1450} (10 g) was dissolved in toluene (250 mL) and water was removed using a Dean−Stark apparatus by heating at reflux for 3 h. After cooling down to room temperature, Ag_2O (3.40 g, 10.35 mmol) and KI (229 mg, 1.38 mmol) were added, followed by *p*-toluenesulfonyl chloride (1.45 g, 7.59 mmol). The suspension was stirred for 18 h at room temperature under an inert atmosphere. After filtration through Celite and evaporation of the filtrate under reduced pressure, the residue was suspended in DCM (200 mL) and washed with H_2O (100 mL) and brine (100 mL). The organic phase was dried over anhydrous Na_2SO_4, filtered, and dried under vacuum. The remaining white wax was used in the next step without further purification. ^1H NMR (400 MHz, 25 °C, $CDCl_3$), δ (ppm): 7.79 (d, $^3J_{HH}$ = 8.3 Hz, 2H, $CH_{Ar}{}^o$), 7.34 (d, $^3J_{HH}$ = 8.3 Hz, 2H, $CH_{Ar}{}^m$), 4.16 (t, $^3J_{HH}$ = 4.8 Hz, 2H, CH_2OTs), 3.70 (t, $^3J_{HH}$ = 4.4 Hz, 2H, $C\underline{H}_2OH$), 3.65−3.55 (m, $C\underline{H}_2CH_2OTs$ + OCH_2CH_2O + $C\underline{H}_2CH_2OH$), 2.66 (bs, 1H, OH), 2.41 (s, 3H, CH_3). ^{13}C NMR (100 MHz, 25 °C, $CDCl_3$), δ (ppm): 144.7 ($C_{Ar}{}^p$), 133.0 ($C_{Ar}{}^i$), 129.8 ($CH_{Ar}{}^m$), 127.9 ($CH_{Ar}{}^o$), 72.5 ($\underline{C}H_2CH_2OH$), 71−70 (PEG), 69.2 ($\underline{C}H_2CH_2OTs$), 68.6 (CH_2OTs), 61.7 (CH_2OH), 21.6 (CH_3). IR (KBr disks), cm^{-1}: 2881, 1465, 1359, 1341, 1279, 1240, 1176, 1145, 1103, 1060, 1016, 946, 920, 841, 774, 663.

*α-Azido-ω-hydroxy-PEG_{1450} (**1**).* α-Tosyl-ω-hydroxy-PEG_{1450} (10 g) was dissolved in DMF (200 mL) and NaN_3 (2.27 g, 34.92 mmol) was added. The suspension was heated to 90 °C and stirred under nitrogen for 18 h. After filtration and evaporation of the solvent under reduced pressure, the solid residue was suspended in DCM (70 mL) and stirred for 1 h. The resulting mixture was filtered, and the filtrate was concentrated under reduced pressure. The product was precipitated upon addition to a 30-fold excess of Et_2O. After centrifugation (4000 rpm, 15 min) and washing twice with Et_2O, a white powder was obtained, that was dried under vacuum (6.12 g). ^1H NMR (400 MHz, 25 °C, $CDCl_3$), δ (ppm): 3.7−3.5 (m, $C\underline{H}_2CH_2N_3$ + OCH_2CH_2O), 3.35 (t, $^3J_{HH}$ = 5.0 Hz, 2H, CH_2N_3), 2.48 (bs, 1H, OH). ^{13}C NMR (100 MHz, 25 °C, $CDCl_3$), δ (ppm): 72.4 ($\underline{C}H_2CH_2OH$), 71−70 (OCH_2CH_2O), 69.9 ($\underline{C}H_2CH_2N_3$), 61.4 (CH_2OH), 50.5 (CH_2N_3). IR (KBr disks), cm^{-1}: 3430, 2889, 2106, 1467, 1343, 1280, 1242, 1115, 1061, 964, 842.

α-Azido-ω-fluorescein-PEG_{1450} (PEG-Flu). α-Azido-ω-hydroxy-PEG_{1450} (1.015 g) was dissolved in dry THF (5 mL).

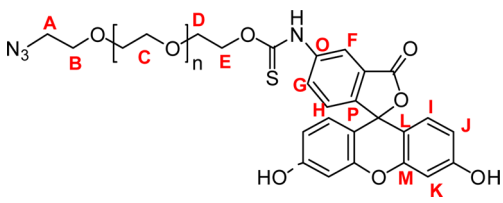

NaH (28 mg, 60 w% in oil, 0.70 mmol) was added, and the suspension was stirred at room temperature for 30 min. FITC (362 mg, 0.84 mmol) was added, and the mixture was stirred at room temperature overnight. After filtration, the filtrate was evaporated under reduced pressure, leading to the target product as an orange wax in 94% yield. ^1H NMR (400 MHz, 25 °C, MeOH-d_4), δ (ppm): 7.88 (s, 1H, f), 7.64 (d, $^3J_{HH}$ = 8.2 Hz, 1H, g), 7.26 (d, $^3J_{HH}$ = 8.2 Hz, 1H, h), 6.69 (m, 4H, j+k), 6.56 (d, $^3J_{HH}$ = 8.8 Hz, 2H, (i), 3.69 (m, 4H, d+e), 3.6−3.5 (m, c+b), 3.37 (t, $^3J_{HH}$ = 4.6 Hz, 2H, a). ^{13}C NMR (100 MHz, 25 °C, MeOH-d_4), δ (ppm): 188.0 (CS), 168.2 (CO), 159.7 (COH), 151.6 (M), 147.7 (P), 134.5 (O), 128−127 (J+G+F), 123.3 (H), 111.5 (I), 108.9 (L), 100.8 (K), 71−65 (C+D+E), 59.3 (B), 48.9 (A). IR (KBr disks), cm^{-1}: 3479, 2874, 2109, 1757, 1614, 1455, 1349, 1294, 1252, 1183, 1108, 949, 848.

α-Azido-ω-methoxy-PEG_{2000} (PEG-OMe). PEG_{2000} monomethyl ether (10.58 g) was dissolved in THF (200 mL). Ag_2O (3.48 g, 15.02 mmol) and KI (332 mg, 2.00 mmol) were added, followed by *p*-toluenesulfonyl chloride (2.29 g, 12.01 mmol). The suspension was stirred for 2 days at room temperature under an inert atmosphere. After filtration and evaporation of the filtrate under reduced pressure, the residue was suspended in H_2O (100 mL) and extracted with DCM (2 × 100 mL). The combined organic phases were washed with H_2O (100 mL) and brine (100 mL), then they were dried over anhydrous Na_2SO_4, filtered, and dried under vacuum. The yellow solid residue obtained was dissolved in DMF (100 mL) and NaN_3 (1.13 g, 17.38 mmol) was added. The suspension was heated to 90 °C and stirred under nitrogen for 18 h. After filtration and evaporation of the solvent under reduced pressure, the solid residue was suspended in DCM (70 mL) and stirred for 1 h. The resulting mixture was filtered, and the filtrate was transferred into a separation funnel and washed with brine (3 × 50 mL). The aqueous phases were re-extracted with DCM (50 mL), and the combined organic phases were dried over anhydrous Na_2SO_4, filtered, and evaporated. The residue was dissolved in MeOH (10 mL) and the solution was slowly added to a 30-fold excess of Et_2O. The obtained suspension was centrifuged (3500 rpm, 10 min) and the precipitate was washed twice with Et_2O. The final solid compound was dried under vacuum (4.81 g). ^1H NMR (400 MHz, 25 °C, $CDCl_3$), δ (ppm): 3.7−3.6 (m, 224H, $C\underline{H}_2CH_2N_3$ + OCH_2CH_2O + $C\underline{H}_2CH_2OMe$), 3.51 (t, $^3J_{HH}$ = 4.6 Hz, 2H, CH_2OMe), 3.35 (t, $^3J_{HH}$ = 5.2 Hz, 2H, CH_2N_3). ^{13}C NMR (100 MHz, 25 °C, $CDCl_3$), δ (ppm): 73−70 (OCH_2CH_2O + $\underline{C}H_2CH_2N_3$), 58.9 (CH_3), 50.6 (CH_2N_3). IR (KBr disks), cm^{-1}: 3434, 2887, 2108, 1653, 1467, 1384, 1359, 1343, 1280, 1242, 1115, 1061, 964, 842.

*α-Azido-ω-tert-butoxycarbonylmethyl-PEG_{1450} (**2**).* α-Azido-ω-hydroxy-PEG_{1450} (5.00 g) was stirred in dry DMF (25 mL) at room temperature until complete dissolution occurred. NaH (461 mg, 60 w% in oil, 11.52 mmol) was added portion-wise at 0 °C, and the resulting suspension was stirred at 0 °C for 30 min. *t*-Butyl bromoacetate (1.13 mL, 7.68 mmol) was added in once, and the mixture was stirred at room temperature under inert atmosphere for 18 h. MeOH (5 mL) was slowly poured into the reactor and the solvents were removed under reduced pressure. The residue was suspended in H_2O (40 mL) and extracted with DCM (3 × 20 mL). The organic phase was dried over anhydrous Na_2SO_4, filtered, and evaporated, and the crude product was purified by column chromatography (SiO_2, DCM/MeOH 95:5, R_f 0.18), leading to the desired compound as a yellow oil (4.22 g). ^1H NMR (400 MHz, 25 °C, $CDCl_3$), δ (ppm): 3.77 (s, 2H, CH_2COO), 3.7−3.5 (m, $C\underline{H}_2CH_2N_3$ + OCH_2CH_2O), 3.36 (t, $^3J_{HH}$ = 4.2 Hz, 2H, CH_2N_3), 1.46 (s, 9H, CH_3). ^{13}C NMR (100 MHz, 25 °C, $CDCl_3$), δ (ppm): 169.1 (CO), 81.5 (CCH_3), 71−70 (OCH_2CH_2O + $\underline{C}H_2CH_2N_3$ + $\underline{C}H_2COO$), 50.7 (CH_2N_3),

DOI: 10.1021/acs.bioconjchem.5b00552
Bioconjugate Chem. 2016, 27, 446−456

Table 3. Amounts of Modified PEGs Reacted with 25 mg of Si−Y or Ho−Y for the Synthesis of the Different Functionalized Particles Used in the Irradiation Studies

particles	PEG-Flu mg/%	PEG-Arg mg/%	PEG-OMe mg/%	aspect
Si-PEG-Flu	25/100	0	0	orange powder
Si-PEG-Flu5%	1.25/5	0	23.75/95	light orange powder
Si-PEG-Flu-Arg	1.25/5	2.5/10	21.25/85	light orange powder
Ho-Flu	25/100	0	0	orange powder

28.1 (CH_3). IR (KBr disks), cm^{-1}: 2869, 2104, 1747, 1456, 1368, 1349, 1299, 1250, 1118, 943, 845.

*α-Azido-ω-carboxymethyl-PEG$_{1450}$ (**3**).* α-Azido-ω-*tert*-butoxycarbonylmethyl-PEG$_{1450}$ (2.15 g) was dissolved in TFA (10 mL), and the mixture was stirred at room temperature for 2 h. After removal of the solvent under vacuum, the product was obtained as a colorless oil (2.04 g) and used without further purification. ^{1}H NMR (400 MHz, 25 °C, $CDCl_3$), δ (ppm): 4.24 (s, 2H, CH_2COO), 3.7−3.5 (m, $C\underline{H}_2CH_2N_3$ + OCH_2CH_2O), 3.42 (t, $^3J_{HH}$ = 4.2 Hz, 2H, CH_2N_3). ^{13}C NMR (100 MHz, 25 °C, $CDCl_3$), δ (ppm): 173.5 (CO), 71−66 (OCH_2CH_2O + $\underline{C}H_2CH_2N_3$ + $\underline{C}H_2COO$), 50.4 (CH_2N_3), IR (KBr disks), cm^{-1}: 3435, 2877, 2537, 2109, 1787, 1669, 1454, 1347, 1298, 1167, 950, 848, 811, 781, 704.

*Resin-Arg$_9$ (**4**).* Fmoc-protected Rink amide resin (500 mg, 0.29 mmol -NH_2) was placed in a reactor. DCM (3 mL) was added, and the suspension was agitated for 30 min by gently bubbling N_2. After removal of the solvent via filtration under vacuum, the resin was deprotected by washing with 20% piperidine in DMF (3 × 3 mL). The resin was washed with DMF (5 × 3 mL). The deprotection was confirmed by ninhydrine test. Separately, Fmoc-Arg(Pbf)−OH (574 mg, 0.89 mmol), HOBt (120 mg, 0.89 mmol), and HBTU (324 mg, 0.85 mmol) were dissolved in DMF (2 mL). DIPEA (0.308 mL, 1.78 mmol) was added and the solution was transferred immediately into the reactor with the resin. The suspension was agitated for 3 h, then it was filtered and the resin was washed with DMF (5 × 3 mL). After confirmation of complete conjugation by Kaiser test, the Fmoc-Arg-resin was reacted with 20% piperidine in DMF (3 × 3 mL) and washed with DMF (5 × 3 mL). The same procedure was repeated 8 more times, replacing HBTU with HATU (325 mg, 0.85 mmol) from the fifth residue of Arg. The peptidyl-resin was used as such for next reactions.

α-Azido-ω-Arg$_9$-PEG$_{1450}$ (PEG-Arg). α-Azido-ω-carboxymethyl-PEG$_{1450}$ (1.10 g), HOBt (94 mg, 0.71 mmol), and HATU (270 mg, 0.71 mmol) were dissolved in DMF (2 mL). DIPEA (247 μL, 1.42 mmol) was added and the solution was transferred into a reactor (filter-syringe) containing **4** (120 mg, 0.071 mmol), washing with DMF (1 mL). The reactor was agitated at room temperature for 18 h. The resin was filtered and washed with DMF (5 × 4 mL), DCM (2 × 4 mL), MeOH (2 × 4 mL), and hexane (2 × 4 mL). The functionalized resin was then suspended in 95:2.5:2.5 TFA/$(i\text{-Pr})_3SiH$/H_2O (5 mL) and agitated at room temperature for 3 h. After filtering, the residue was washed with TFA (3 × 1 mL) and the combined filtrates were concentrated under vacuum, precipitated in Et_2O (10 mL), and centrifuged (4000 rpm, 15 min, 20 °C). The obtained white solid was further washed/centrifuged in Et_2O (3 × 10 mL) and dried under vacuum (69 mg). ^{1}H NMR (400 MHz, 25 °C, D_2O), δ (ppm): 4.19 (bm, 9H, CH), 4.01 (bs, 2H, $COCH_2O$), 3.8−3.4 (PEG), 3.38 (bm, 2H, CH_2N_3), 3.09 (bm, 18H, $CHCH_2CH_2C\underline{H}_2$), 1.71 (bm, 18H, $CHC\underline{H}_2$), 1.53 (bm, 18H, $CHCH_2C\underline{H}_2$). ^{13}C NMR (100 MHz, 25 °C, $CDCl_3$), δ (ppm): 176.1 ($CONH_2$), 173.5 (CONH), 156.7 (C═N), 71−69 (OCH_2CH_2O + $\underline{C}H_2CH_2N_3$), 69.2 ($CO\underline{C}H_2O$), 53.3 (CH), 50.1 (CH_2N_3), 40.5 ($CHCH_2CH_2\underline{C}H_2$), 28.1 ($CH\underline{C}H_2$), 24.4 ($CHCH_2\underline{C}H_2$). IR (KBr disks), cm^{-1}: 3350, 3188, 2947, 2475, 2110, 1661, 1543, 1451, 1353, 1192, 1111, 1049, 864, 589.

Preparation of Functionalized Si- and Ho-Nanoparticles. *N-(Prop-2-yn-1-yl)-N-(3-(trimethoxysilyl)propyl)-prop-2-yn-1-amine.* CaH_2 (3.62 g, 85.90 mmol) was suspended in dry THF (60 mL) under nitrogen. (3-Aminopropyl)trimethoxysilane (3.00 mL, 17.18 mmol) was added, followed after 15 min stirring by propargyl bromide (4.21 mL, 80 wt % solution, 37.80 mmol). The suspension was stirred at room temperature for 18 h, then the solvent was evaporated under reduced pressure and the residue was suspended in hexane (50 mL), stirred for 30 min, and filtered. The filtrate was dried under vacuum, leading to the product as yellow oil (824 mg, 19%). ^{1}H NMR (400 MHz, 25 °C, D_2O), δ (ppm): 3.54 (s, 9H, CH_3), 3.41 (d, $^4J_{HH}$ = 2.4 Hz, 4H, $C\underline{H}_2CCH$), 2.50 (t, $^4J_{HH}$ = 7.4 Hz, 2H, $NC\underline{H}_2CH_2$), 2.20 (t, $^4J_{HH}$ = 2.4 Hz, 2H, CH), 1.56 (m, 2H, $NCH_2C\underline{H}_2$), 0.63 (m, 2H, $SiCH_2$). ^{13}C NMR (100 MHz, 25 °C, $CDCl_3$), δ (ppm): 78.8 (C), 72.9 (CH), 55.6 ($N\underline{C}H_2CH_2$), 50.5 (CH_3), 42.0 ($\underline{C}H_2CCH$), 20.6 ($NCH_2\underline{C}H_2$), 6.6 ($SiCH_2$). IR (KBr disks), cm^{-1}: 3293, 2943, 2840, 1457, 1349, 1328, 1192, 1084, 982, 898, 818, 782.

Si−Y. EtOH (200 mL) was sonicated for 10 min, then tetraethyl orthosilicate (5 mL) was added and sonication was continued for 20 min. NH_4OH (5 mL) and H_2O (7.5 mL) were added and the mixture was left under sonication for 5 h. Propargylaminosilane (500 mg) in EtOH (5 mL) was added to the resulting suspension under vigorous stirring, which was continued for 18 h. The suspension was then centrifuged (3500 rpm, 20 min) and washed/centrifuged in EtOH (2×, 3 drops of brine per 10 mL of solvent) and H_2O (3×, 3 drops of brine per 10 mL of solvent). The alkynylated Si-nanoparticles (754 mg) were finally freeze-dried.

Ho−Y.[28] Ho_2O_3 (50 mg) was suspended in AcOH (20 mL) and stirred at room temperature for 18 h. After removal of the solvent under reduced pressure, the particles were suspended in H_2O (50 mL), EtOH (200 mL), and NH_4OH (2.5 mL) and sonicated for 1 h. A solution of propargylaminosilane (5 mg) in EtOH (1 mL) was added slowly through a syringe-pump (0.125 mL h^{-1}) under vigorous stirring, and the resulting suspension was concentrated, centrifuged (4000 rpm, 20 min, 25 °C) and washed/centrifuged in EtOH (3 × 10 mL). The alkynylated Ho-nanoparticles were dried under vacuum (47 mg).

General Method for the Preparation of Functionalized Nanoparticles. Si−Y or Ho−Y nanoparticles (25 mg) were suspended in THF (1 mL) and Et_3N (1 mL) together with 25 mg of a proper mixture of desired PEGs (Table 3). The suspension was sonicated for 30 min, then a fresh solution of $(PPh_3)_3CuBr$ (6 mg, 0.0525 mmol) in THF (1 mL) was added

DOI: 10.1021/acs.bioconjchem.5b00552
Bioconjugate Chem. 2016, 27, 446−456

and the mixture was vigorously stirred at room temperature for 18 h. After centrifugation (4000 rpm, 15 min), the solid residue was washed/centrifuged with THF (2 × 10 mL), EtOH (2 × 10 mL), and H_2O (2 × 10 mL). The residue was then suspended in H_2O (10 mL) and dialyzed against MeOH/H_2O 1:1 (1×) and H_2O (2×). The resulting suspension was freeze-dried.

Neutron Activation Experiments. *Irradiation of SiO_2 Particles.* 50 mg of SiO_2 functionalized nanoparticles were placed in polyethylene vials, which were wrapped in thin polyethylene foil and inserted in a high density polyethylene (rabbit) container. The pneumatic irradiation system of the HOR (Hoger Onderwijs Reactor) reactor at the TU Delft was used for irradiations of 2, 4, 6, 8, and 10 h. This facility has nominal thermal neutron flux of 5.01×10^{16} n m^{-2} s^{-1}, epithermal neutron flux of 8.08×10^{14} n m^{-2} s^{-1}, and fast neutron flux of 3.52×10^{15} n m^{-2} s^{-1}. All samples were left to decay for at least 2 weeks to ensure that all activity due to impurities or silica itself is gone before analysis.

Irradiation of Ho_2O_5 Nanoparticles. 5 mg of functionalized nanoparticles were irradiated for 2 h in the HOR (Hoger Onderwijs Reactor) reactor at the TU Delft in the same irradiation facility as described above and using the irradiation procedure. The activity of these particles was 0.3 GBq immediately after irradiation. In this case, the particles were left to decays for 4 days before proceeding with the analysis. The gamma dose of the pneumatic facility was determined to be 265 ± 3 kGy h^{-1} using Harwell 3042 dosimeters.

Cell Experiments. *Preparation of Silica Nanoparticles Suspensions for in Vitro Studies.* Suspensions were prepared by dissolving 1 mg of freeze-dried nanoparticles (Si-PEG-Flu5%, Si-PEG-Flu-Arg, Si-PEG-Flu-Arg-IRR2h or Si-PEG-Flu-Arg-IRR4h) in 10 mL of complete cell culture medium. The solutions were then exposed to 2 h of ultrasound followed by hand shake to promote the complete dispersion of the silica nanoparticles in the cell medium. Finally, the samples were sterilized by filtration using Acrodisc sterile syringe filters with 0.22 μm Supor membrane (Pall Corporation).

Cell Culture Conditions. HeLa human cervical carcinoma epithelial cells were acquired from ATCC and grown as monolayer cultures in a 50/50 mixture of Dulbecco's modified Eagle's medium and Ham's F10 (Lonza, BioWhittaker) supplemented with 10% fetal bovine serum and 0.5% (v/v) penicillin-streptomycin (Sigma-Aldrich). Cell cultures were prepared from deep frozen stock vials and seeded in 25 cm^2 culture bottles (Cellstar, Greigner Bio-One). Cells were incubated under standard cell culture conditions (37 °C, 5% CO_2, and 95% humidity) and maintained until subconfluence was reached (70−80%).

Internalization and Intracellular Localization. 1×10^5 HeLa cells were seeded in 20 × 20 mm borosilicate glass slides placed inside 6-well plates (Corning) and were allowed to attach overnight. Then, cells were incubated with the previously prepared silica nanoparticles suspensions (see above) at a final concentration of 100 μg mL^{-1} during 1 h at 37 °C. To determine the subcellular location and colocalization of Si-PEG-Flu-Arg with endocytic compartments, HeLa cells were incubated for 1 h at 37 °C with Si-PEG-Flu-Arg, followed by replacement of the cell medium with a 50 nM solution of Lysotracker Red DND-99 (Life Technologies) in cell culture medium at 37 °C for 30 min. After the incubation period, cell slides were washed twice with PBS and fixed with 3.7% formaldehyde in PBS for 15 min. Slides were washed again thrice with PBS and mounted with DAPI Vectashield (Vector Laboratories). Cell slides were stored in the darkness at 4 °C before confocal microscopy. Images were captured with a Carl Zeiss LSM710 microscope and were superimposed to determine the colocalization of the nanocarriers with the lysosomes.

■ ASSOCIATED CONTENT

Supporting Information

The Supporting Information is available free of charge on the ACS Publications website at DOI: 10.1021/acs.bioconjchem.5b00552.

TEM images, UV−vis and fluorescence spectra, data from spectroscopic analyses, data from thermogravimetric analyses (PDF)

■ AUTHOR INFORMATION

Corresponding Author

*E-mail: k.djanashvili@tudelft.nl. Phone: +31 15 2785092.

Notes

The authors declare no competing financial interest.

■ ACKNOWLEDGMENTS

This work was performed in the framework of the EU COST Action TD1004, "Theranostics Imaging and Therapy: an Action to Develop Novel Nanosized Systems for Imaging-Guided Drug Delivery" and supported by China Scholarship Council (W.Z.) and The Netherlands Organization for Scientific Research (K.D. and J.M., NWO Veni grant-722.012.009). Dr. Alberto Fraccarollo (Department of Science and Technological Innovation, Università del Piemonte Orientale, Alessandria, Italy) is gratefully acknowledged for the molecular modeling design of the SiO_2 and Ho_2O_3 nanoparticles.

■ REFERENCES

(1) Schindler, T. H. (2015) Positron-Emitting Myocardial Blood Flow Tracers and Clinical Potential. *Prog. Cardiovasc. Dis. 57*, 588−606.

(2) Jacobson, O., Kiesewetter, D. O., and Chen, X. (2015) Fluorine-18 Radiochemistry, Labeling Strategies and Synthetic Routes. *Bioconjugate Chem. 26*, 1−18.

(3) Ghotbi, A. A., Kjaer, A., and Hasbak, P. (2014) Review: comparison of PET rubidium-82 with conventional SPECT myocardial perfusion imaging. *Clin. Physiol. Funct. Imaging 34*, 163−170.

(4) Psimadas, D., Georgoulias, P., Valotassiou, V., and Loudos, G. (2012) Molecular Nanomedicine Towards Cancer: In-111-Labeled Nanoparticles. *J. Pharm. Sci. 101*, 2271−2280.

(5) Sogbein, O. O., Pelletier-Galarneau, M., Schindler, T. H., Wei, L., Wells, R. G., and Ruddy, T. D. (2014) New SPECT and PET radiopharmaceuticals for imaging cardiovascular disease. *BioMed Res. Int. 2014*, 1−24.

(6) Wright, C. L., Zhang, J., Tweedle, M. F., Knopp, M. V., and Hall, N. C. (2015) Theranostic Imaging of Yttrium-90. *BioMed Res. Int. 2015*, 1−11.

(7) Goyal, J., and Antonarakis, E. S. (2012) Bone-targeting radiopharmaceuticals for the treatment of prostate cancer with bone metastases. *Cancer Lett. 323*, 135−146.

(8) Imam, S. K. (2001) Advancements in cancer therapy with alpha-emitters: A review. *Int. J. Radiat. Oncol., Biol., Phys. 51*, 271−278.

(9) Rubini, G., Nicoletti, A., Rubini, D., and Asabella, A. N. (2014) Radiometabolic Treatment of Bone-Metastasizing Cancer: From (186)Rhenium to (223)Radium. *Cancer Biother.Radiopharm. 29*, 1−11.

DOI: 10.1021/acs.bioconjchem.5b00552
Bioconjugate Chem. 2016, 27, 446−456

(10) Srivastava, S. C. (2014) Enabling simultaneous imaging and treatment with the theragnostic radionuclide Tin-117 m. *Nucl. Med. Biol. 41*, 640−640.
(11) Wyszomirska, A. (2012) Iodine-131 for therapy of thyroid diseases. Physical and biological basis. *Nucl. Med. Rev. 15*, 120−3.
(12) Hruby, M., Pouckova, P., Zadinova, M., Kucka, J., and Lebeda, O. (2011) Thermoresponsive polymeric radionuclide delivery system-An injectable brachytherapy. *Eur. J. Pharm. Sci. 42*, 484−488.
(13) Banerjee, S., Pillai, M. R. A., and Knapp, F. F. (2015) Lutetium-177 Therapeutic Radiopharmaceuticals: Linking Chemistry, Radiochemistry, and Practical Applications. *Chem. Rev. 115*, 2934−2974.
(14) Nijsen, J. F. W., Zonnenberg, B. A., Woittiez, J. R. W., Rook, D. W., Swildens-van Woudenberg, I. A., van Rijk, P. P., and Schip, A. D. V. (1999) Holmium-166 poly lactic acid microspheres applicable for intra-arterial radionuclide therapy of hepatic malignancies: effects of preparation and neutron activation techniques. *Eur. J. Nucl. Med. Mol. Imaging 26*, 699−704.
(15) Vente, M. A. D., Nijsen, J. F. W., de Roos, R., van Steenbergen, M. J., Kaaijk, C. N. J., Koster-Ammerlaan, M. J. J., de Leege, P. F. A., Hennink, W. E., van het Schip, A. D., and Krijger, G. C. (2009) Neutron activation of holmium poly(L-lactic acid) microspheres for hepatic arterial radioembolization: a validation study. *Biomed. Microdevices 11*, 763−772.
(16) Smits, M. L. J., Nijsen, J. F. W., van den Bosch, M., Lam, M., Vente, M. A. D., Huijbregts, J. E., van het Schip, A. D., Elschot, M., Bult, W., and de Jong, B. A. (2010) Holmium-166 radioembolization for the treatment of patients with liver metastases: design of the phase I HEPAR trial. *J. Exp. Clin. Cancer Res. 29*, 70.
(17) Bridot, J.-L., Faure, A.-C., Laurent, S., Riviere, C., Billotey, C., Hiba, B., Janier, M., Josserand, V., Coll, J.-L., Vander Elst, L., et al. (2007) Hybrid gadolinium oxide nanoparticles: Multimodal contrast agents for in vivo imaging. *J. Am. Chem. Soc. 129*, 5076−5084.
(18) Tok, A. I. Y., Su, L. T., Boey, F. Y. C., and Ng, S. H. (2007) Homogeneous precipitation of Dy_2O_3 nanoparticles-effects of synthesis parameters. *J. Nanosci. Nanotechnol. 7*, 907−915.
(19) Briley-Saebo, K., Bjornerud, A., Grant, D., Ahlstrom, H., Berg, T., and Kindberg, G. M. (2004) Hepatic cellular distribution and degradation of iron oxide nanoparticles following single intravenous injection in rats: implications for magnetic resonance imaging. *Cell Tissue Res. 316*, 315−323.
(20) Jokerst, J. V., Lobovkina, T., Zare, R. N., and Gambhir, S. S. (2011) Nanoparticle PEGylation for imaging and therapy. *Nanomedicine 6*, 715−728.
(21) Farokhzad, O. C., and Langer, R. (2009) *ACS Nano 3*, 16−20.
(22) Karakoti, A. S., Das, S., Thevuthasan, S., and Seal, S. (2011) PEGylated Inorganic Nanoparticles. *Angew. Chem., Int. Ed. 50*, 1980−1994.
(23) Mahou, R., and Wandrey, C. (2012) Versatile Route to Synthesize Heterobifunctional Poly(ethylene glycol) of Variable Functionality for Subsequent Pegylation. *Polymers 4*, 561−589.
(24) Futaki, S., Suzuki, T., Ohashi, W., Yagami, T., Tanaka, S., Ueda, K., and Sugiura, Y. (2001) Arginine-rich peptides - An abundant source of membrane-permeable peptides having potential as carriers for intracellular protein delivery. *J. Biol. Chem. 276*, 5836−5840.
(25) Wunderbaldinger, P., Josephson, L., and Weissleder, R. (2002) Tat peptide directs enhanced clearance and hepatic permeability of magnetic nanoparticles. *Bioconjugate Chem. 13*, 264−268.
(26) Stober, W., Fink, A., and Bohn, E. (1968) Controlled Growth Of Monodisperse Silica Spheres In Micron Size Range. *J. Colloid Interface Sci. 26*, 62−69.
(27) Burglova, K., Moitra, N., Hodacova, J., Cattoen, X., and Man, M. W. C. (2011) Click Approaches to Functional Water-Sensitive Organotriethoxysilanes. *J. Org. Chem. 76*, 7326−7333.
(28) Zhang, W. Y., Martinelli, J., Mayer, F., Bonnet, C. S., Szeremeta, F., and Djanashvili, K. (2015) Molecular architecture control in synthesis of spherical Ln-containing nanoparticles. *RSC Adv. 5*, 69861−69869.
(29) Gujadhur, R., and Venkataraman, D. (2001) Synthesis of diaryl ethers using an easy-to-prepare, air-stable, soluble copper(I) catalyst. *Synth. Commun. 31*, 2865−2879.
(30) Lal, S., and Diez-Gonzalez, S. (2011) CuBr(PPh3)(3) for Azide-Allkyne Cycloaddition Reactions under Strict Click Conditions. *J. Org. Chem. 76*, 2367−2373.
(31) Bouzide, A., LeBerre, N., and Sauve, G. (2001) Silver(I) oxide-mediated facile and practical sulfonylation of alcohols. *Tetrahedron Lett. 42*, 8781−8783.
(32) Mumper, R. J., Ryo, U. Y., and Jay, M. (1991) Neutron-Activated Holmium-166-Poly (L-Lactic Acid) Microspheres - A Potential Agent For The Internal Radiation-Therapy Of Hepatic-Tumors. *J. Nucl. Med. 32*, 2139−2143.

DOI: 10.1021/acs.bioconjchem.5b00552
Bioconjugate Chem. 2016, 27, 446−456